ACS Catalysis

Research Article

pubs.acs.org/acscatalysis

Strong Metal–Support Interactions Enhance the Activity and Durability of Platinum Supported on Tantalum-Modified Titanium Dioxide Electrocatalysts

Amod Kumar and Vijay Ramani*

Center for Electrochemical Science and Engineering, Department of Chemical and Biological Engineering, Illinois Institute of Technology, 10 West 33rd Street, Chicago, Illinois 60616, United States

Supporting Information

ABSTRACT: Rutile phase tantalum-modified titanium oxide ($Ta_{0.3}Ti_{0.7}O_2$) was synthesized and studied using electrochemical and spectroscopic methods to evaluate its efficacy as a corrosion-resistant electrocatalyst support material. A 20 wt % Pt supported on $Ta_{0.3}Ti_{0.7}O_2$ catalyst was prepared and compared in terms of activity and stability against a 20 wt % Pt supported on Vulcan XC-72R carbon catalyst (20% Pt/C; synthesized in-house) and a 46 wt % Pt/C commercially sourced catalyst (Tanaka KK). Catalysts 20% Pt/$Ta_{0.3}Ti_{0.7}O_2$, 20% Pt/C, and 46% Pt/C possessed electrochemically active surface areas (ECSAs) of 60, 57, and 65 $m^2\ g^{-1}$, respectively, and mass activities for the oxygen reduction reaction (at 0.9 V vs RHE) of 185, 148, and 224 mA mg^{-1}_{Pt}, respectively, as evaluated in an operating polymer electrolyte fuel cell. Accelerated stability tests (ASTs) were performed on membrane electrode assemblies (MEAs) in an operating fuel cell to investigate both support and platinum catalyst stability. The loss in voltage at a current density of 0.4 Acm^{-2} after 10 000 support stability AST cycles was only 23 mV for 20% Pt/$Ta_{0.3}Ti_{0.7}O_2$, over an order of magnitude lower than the losses observed in 20% Pt/C and 46% Pt/C (~330 mV). Although the latter loss would correspond to catastrophic fuel cell and stack failure, the former is well within the limits of system tolerance. Post-mortem transmission electron microscopy (TEM) analyses of the electrocatalyst recovered from cycled MEAs confirmed the excellent stability of Pt nanoparticles supported on $Ta_{0.3}Ti_{0.7}O_2$. The average Pt particle size increased by ~20% in 20% Pt/$Ta_{0.3}Ti_{0.7}O_2$, as compared with a doubling in size in the case of 20% Pt/C and a near tripling in size in 46% Pt/C. The existence of strong metal–support interactions in 20% Pt/$Ta_{0.3}Ti_{0.7}O_2$ was ascertained from the X-ray absorption near edge structure analysis. The number of unfilled d states in 20% Pt/$Ta_{0.3}Ti_{0.7}O_2$ was found to be ~1.47, which was lower than the value of ~1.60 found in both the carbon-supported Pt catalysts. The decrease in the number of unfilled d states confirmed electron donation from the $Ta_{0.3}Ti_{0.7}O_2$ support to the Pt atoms, resulting in an increased electron density on Pt. This interaction enhanced both electrocatalytic activity and catalyst stability, as evidenced by the results above.

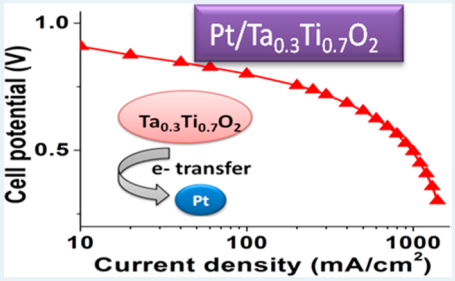

KEYWORDS: *corrosion-resistant electrocatalyst support, fuel cell, carbon corrosion, potential cycling, Ta-modified TiO_2, strong metal–support interactions*

1. INTRODUCTION

Polymer electrolyte fuel cells (PEFCs) are electrochemical energy conversion devices with applications in the automotive, residential, back-up power, military, portable, and space sectors. However, PEFC technology has several underlying problems (lifetime, reliability, and cost) that need to be resolved as a prerequisite for large-scale commercialization. Among these, the lifetime issue is regarded as critical.[1] PEFC lifetime is a function of the durability of its primary component parts (electrocatalyst, electrolyte, and diffusion media) and resultant interfaces, which are exposed during operation to an aggressive combination of two or more of the following: low pH, severe oxidizing/reducing conditions, excess/insufficient hydration, temperature excursions, and high electrochemical potentials.[1,2] Component lifetime is heavily influenced by various operational factors, such as abrupt changes in load and cell start-up/shutdown; an adverse manifestation of these factors can accelerate component degradation. Catalyst durability during extended operation remains a key challenge to developing PEFCs with acceptable lifetime, especially for applications in the automotive sector. Platinum supported on high-surface-area carbon (Pt/C) is widely used as an electrocatalyst in PEFCs because of its relatively high activity for the oxygen reduction reaction (ORR). However, loss in active platinum surface area occurs during fuel cell operation as a consequence of catalyst and support degradation. Loss in Pt surface area is associated with the growth in platinum nanoparticle crystal size as a result of the following mechanisms: (i) platinum dissolution and redeposition via the Ostwald ripening process, (ii) coalescence of platinum particles via migration on the carbon support, and

Received: January 24, 2014
Revised: March 31, 2014
Published: April 2, 2014

   dx.doi.org/10.1021/cs500116h | ACS Catal. 2014, 4, 1516–1525

(iii) platinum particle detachment and agglomeration induced by carbon support corrosion.[3]

The corrosion of carbon in acidic electrolytes occurs as[4]

$$C + H_2O \rightarrow CO_2 + 4H^+ + 4e^-$$
$$E^o = 0.207 \text{ V vs RHE} \quad [1]$$

This reaction is thermodynamically feasible at the potentials at which the PEFC cathode operates (typically 0.6−1.0 V vs RHE) but occurs at very low rates in this potential range as a result of the inherently slow kinetics.[5] During fuel cell startup and shutdown in automotive applications, the cathode potential undergoes excursions of up to 1.5 V for time periods corresponding to the residence time of the mixed fuel-air front in the anode flow channels. Likewise, under conditions of fuel starvation during operation, similar excursions in potential are seen at the anode. At these high potentials, the carbon corrosion reaction is significantly accelerated (as a result of the exponential dependence of the electrochemical rate constant on potential), leading to irreversible carbon loss at the electrode.[5b,6] Electrochemical corrosion of carbon causes electrical isolation of the catalyst particles as they are separated from the support and also leads to aggregation of catalyst particles. Both of these outcomes result in a decrease in the electrochemically active surface area (ECSA) and mass activity of the catalyst. There is also an increase in surface hydrophilicity due to surface oxidation, which promotes condensed phase mass transport limitations resulting from water retention within the pores of the catalyst. The presence of Pt can accelerate the carbon support corrosion rate.[6b,7]

The best way to eliminate the issue of support corrosion in PEFCs is to develop alternate corrosion-resistant catalyst supports. Numerous candidates, including a variety of carbon nanostructures,[8] metal oxides,[9] conducting polymers,[10] and hybrid materials,[11] have been exhaustively researched over the past few decades in an attempt to develop novel PEFC catalyst supports. Transition metal nitrides such as TiN possess high corrosion-resistance and high conductivity, making them excellent support candidates. However, the TiN undergoes passivation under electrochemical conditions, leading to a loss of conductivity.[12] Transition metal carbides/borides, such as titanium carbide, boron carbide, silicon carbide, and titanium boride, have been shown to exhibit high conductivity and stability.[9,13] Electrocatalysts using titanium carbide as a support have been shown to have good catalytic activity,[14] although they suffer from low surface area, which prevents high dispersion of metal catalyst.[15] Various metal oxides/mixed oxides have been investigated as substitutes for carbon for low-temperature fuel cell catalysts, including SnO_2,[16] ITO,[17] WOx,[18] TiO_2,[19] RuO_2,[19c,20] and SiO_2.[20b,c,21] Some of these metal oxide supports have been shown to act as cocatalysts that enhance the activity of the supported electrocatalyst. Titanium oxide-based materials have garnered special attention because of their excellent corrosion resistance in various electrolyte media.[19c,22] The high corrosion resistance and electrochemical stability demonstrated by titanium oxides even at low pH has encouraged studies of these materials in fuel cells.[22a,c] Titania has the added advantage of being cost-effective, nontoxic, and readily available.[23] However, because of the low electron conductivity of TiO_2, a Pt supported on bare TiO_2 electrocatalyst is deemed unsuitable. The poor performance of this material in an electrochemical environment has been shown previously.[24]

Titania can exist in three main crystallographic forms: rutile, anatase, and brookite. At room temperature, the rutile phase of TiO_2 has a band gap of 3.0 eV and the anatase phase has a band gap of 3.2 eV.[25] Because of this difference in their band gaps, the conductivity of the rutile phase of TiO_2 is higher than that of the anatase phase.[25,26] Stoichiometric titania is resistive, and the presence of Ti^{3+} ions is essential for electronic conductivity. Ti^{3+} ions can be generated by (i) creating oxygen deficiencies by heating TiO_2 in a reducing atmosphere (to obtain TiO_{2-x} or Ti_nO_{2n-1}), and (ii) introducing dopants. Magneli-phase titania, which can be obtained by annealing TiO_2 at high temperatures of 850 °C, exhibits high conductivity (~1000 S/cm) as a result of the presence of induced oxygen defects.[19b,27] However, substoichiometric titania becomes stoichiometic when exposed to fuel cell conditions, with a resistive TiO_2 layer formed at the three-phase-reaction interface.[19b]

Doping rutile titania with metals such as Zr,[28] Hf,[29] V,[30] Nb,[22b,31] Ta,[32] Cr,[33] Mo,[34] W,[22e] Ru,[35] Os,[36] and Sn[37] can increase its electron conductivity, and several such doped titania materials, such as $Nb_{0.06}Ti_{0.94}O_2$,[22d] 10 mol % Nb-doped TiO_2,[31a] $Ta_{0.3}Ti_{0.7}O_2$,[32] $Ti_{0.7}Mo_{0.3}O_2$,[34] $Ti_{0.7}W_{0.3}O_2$,[22e] and $Ti_{0.7}Ru_{0.3}O_2$,[35b] have been previously evaluated for electrochemical stability. Numerous studies have been carried out using $Nb_xTi_{1-x}O_2$, and this support and derivative electrocatalysts have been shown to possess high activity and stability. Park and Seol[31c] reported an increase in electron conductivity from 10^{-6} to 0.1 S/cm of Nb-doped TiO_2 prepared by hydrothermal synthesis and annealed at 400 °C. Huang et al.[22b] reported the ambient temperature electron conductivity of niobium-doped titania ($Nb_{0.25}Ti_{0.75}O_2$) prepared by a template-assisted sol−gel method and annealed at 900 °C to be around 1.11 S/cm and also reported comparable catalytic activities for 33.8 wt % $Pt/Nb_{0.25}Ti_{0.75}O_2$ and 20 wt % Pt/C catalysts (the latter sourced from E-TEK). Both catalysts were found to have a mass specific activity (at 0.85 V vs RHE) of ~30 mA/mg_{Pt}, far lower than those reported for state-of-the-art benchmark catalysts that possess mass activity values of ~200 mA/mg_{Pt}.[38]

After accelerated durability tests (potential cycling from 0.6 to 1.4 V at 50 mV/s for 2500 cycles), the activity of 33.8 wt % $Pt/Nb_{0.25}Ti_{0.75}O_2$ was reported to be 10 times higher than that of Pt/C as a result of carbon corrosion in the 20 wt % Pt/C catalyst; however, the absolute value of the mass activity was still low, as stated above. Wang et al.[22d] measured the conductivity of $Nb_xTi_{1-x}O_2$ and obtained a value of 7.7×10^{-5} S/cm at room temperature. The low reduction temperature (400 °C) employed during synthesis of these materials likely resulted in the lower electron conductivity obtained in this case. Similarly, Sun et al. reported higher activity and stability of Pt supported on Nb-TiO_2 mesoporous spheres when compared with commercial E-TEK Pt/C.[39] Pt/Nb-TiO_2 catalysts were reported to possess mass activities (at 0.9 V vs RHE) between 82 and 92 mA/mg_{Pt}, much lower than the state of the art benchmark catalysts. (As a general note, in many studies, the internal benchmark mass activities fall far short of what is considered to be acceptable: a value around 200 mA/mg_{Pt} at the very least. Thus, although new catalysts are shown to have mass activities "superior" to internal benchmarks, the merit of this claim is frequently questionable, given the suboptimal benchmark employed. A typical claim is that the comparison was performed under similar conditions using similar equipment; however, this cannot excuse having a larger than 10% or so variance with the best reported benchmarks, given that the benchmarking procedures have been carefully

dx.doi.org/10.1021/cs500116h | ACS Catal. 2014, 4, 1516−1525

documented.[38,40]) After 30 000 cycles of potential sweeps from 0.6 to 1.4 V vs RHE, Pt/Nb-TiO_2 retained only ∼40% of its initial ECSA, although it was found to be more durable than the Pt/C ETEK catalyst (which retained only 19% of its initial ECSA). Ho et al.[34] reported high stability of 20% Pt/$Ti_{0.7}Mo_{0.3}O_2$ during potential cycling from 0 to 1.1 V after 5000 cycles. This protocol, however, does not account for the high potential excursions (∼1.5 V) experienced during start-up of an automotive PEFC. Binary oxides of $Ru_xTi_{1-x}O_2$ were synthesized by Haas et al.[35a] for application as a catalyst support for PEFC; however, no stability results were carried out.

Tantalum-modified TiO_2 has previously been used as a thick film gas sensor,[41] nanowires for solar cells,[42] and for varistor applications[43] and possesses electrical conductivities of as high as $\sim 10^3$ S/cm when synthesized as an epitaxial thin film. Our previous work[32] reported on the electrochemical properties of Ta-modified TiO_2 measured in a rotating disk electrode (RDE) setup. The $Ta_{0.3}Ti_{0.7}O_2$ support displayed very high electrochemical durability; the loss in capacitance was ∼12% compared with a carbon benchmark, which showed a >100% change in pseudocapacitance over 10 000 AST cycles (1.0−1.5 V vs RHE at a scan rate of 500 mV/s in a 0.1 M $HClO_4$ electrolyte at 25 °C). The 20% Pt/$Ta_{0.3}Ti_{0.7}O_2$ possessed promising mass activity (at 0.9 V vs RHE; 62 mA/mg_{Pt}) for ORR in RDE. In this study, we evaluate and benchmark the mass and specific activity, ECSA, performance and stability (loss in mass/specific activities, ECSA, and performance upon exposure to realistic ASTs) of the Pt/$Ta_{0.3}Ti_{0.7}O_2$ catalyst in situ in an operating PEFC.

There have been several reports on the unique ability of TiO_2 and doped TiO_2 supports[34,35b,44] to alter the electronic structure of supported platinum. This phenomenon has been classified under "strong metal−support interactions" (SMSI) and has been shown to enhance both chemical stability and oxygen reduction reaction (ORR) activity.[45] In this study, we have interrogated the 20% Pt/$Ta_{0.3}Ti_{0.7}O_2$ catalyst using X-ray absorption spectroscopy for evidence of SMSI, and we investigate the role of such interactions in enhancing catalytic activity and catalyst stability.

2. EXPERIMENTAL SECTION

2.1. Synthesis of Support and Catalyst. Ta-modified TiO_2 supports were synthesized using a sol−gel technique using a procedure modified from those available in the literature.[32,41,42] Briefly, alkoxides of tantalum and titanium as precursors were used in conjunction with a high water/alkoxide ratio. A 3.0 mL portion of 11.57 mmol of tantalum ethoxide [$Ta(OEt)_5$] was mixed with 8 mL of 27 mmol of titanium isopropoxide [$Ti(OiPr)_4$] in 92 mL of absolute ethanol, added dropwise to an ethanol/water 1:1 solution, and the mixture was stirred for 4 h. The resultant mixture was centrifuged and then washed with deionized water and acetone, followed by drying in an oven at 60 °C for 8 h. This resulted in the formation of 30% Ta-modified TiO_2. As discussed previously,[32] this formulation resulted in adequate electron conductivity (∼0.2 S/cm) for support while also ensuring complete incorporation of Ta inside the TiO_2 structure. The resultant powder was annealed at 850 °C in a tube furnace in a reducing atmosphere of 4% H_2 in argon for 3 h. An argument for using a reducing atmosphere for efficient large dopant (Ta) incorporation is discussed here.[46]

The 20% Pt supported on carbon and 20% Pt supported on $Ta_{0.3}Ti_{0.7}O_2$ were prepared by a modified incipient wetness technique. The details of Pt deposition on $Ta_{0.3}Ti_{0.7}O_2$ have also been described elsewhere.[32,47] A similar procedure was adopted to prepare 20% Pt/C. Briefly, 0.1327 g of $H_2PtCl_6 \cdot 6H_2O$ was added to 30 mL of ethanol, and the mixture was stirred for 30 min. A 0.2 g portion of support (Vulcan carbon/$Ta_{0.3}Ti_{0.7}O_2$) was added to the mixture, and the resultant suspension was sonicated for 1 h. The suspension was then stirred continuously at 60 °C to evaporate the solvent. The resultant slurry was dried completely at 80 °C and ground to a fine powder using a mortar and pestle. To ensure complete reduction of the Pt precursor to metallic platinum, the powder was placed in a ceramic boat and heated in a tube furnace at 120 °C under flowing 4% H_2/Ar. The resultant 20% Pt/$Ta_{0.3}Ti_{0.7}O_2$ and 20% Pt/C catalysts were tested and compared against a commercially available benchmark 46% Pt/C (TKK) that has gained wide acceptance in industry.

2.2. Microstructure and Electronic Properties. Transmission electron microscopy (TEM) micrographs were obtained using a JEOL 3010F electron microscope operating at 300 kV. X-ray absorption spectra (XAS) were recorded at the Pt L2 and L3 edges in transmission mode at the Materials Research Collaborative Access Team (MRCAT) beamline, Sector 10 μ_B,[48] at the Advanced Photon Source at Argonne National Laboratory. The water cooled Si (111) monochromator was operated in step scan mode with an entire spectrum collected in 20 min. An appropriate metal foil (Pt metal) was used for energy calibration. The powder samples (between 5 to 20 mg) were first ground into a fine powder and then evenly spread on kapton tape and folded; measurements were made at room temperature. The total amount of the sample was adjusted to reach the optimum absorption thickness ($\Delta\mu x$ = 1.0; $\Delta\mu$ is the absorption edge and x is the thickness of the sample) so that the proper edge jump step could be achieved during the measurements. Higher harmonics were eliminated by detuning the double-crystal Si(111) monochromator. Three gas-filled ionization chambers were used in series to measure the intensities of the incident beam (I_0), the beam transmitted by the sample (I_t), and the beam subsequently transmitted by the reference foil (I_r). The third ion chamber was used in conjunction with the reference sample, which was a Pt foil for Pt LII and LIII-edge measurements. X-ray absorption near edge spectroscopy (XANES) data were processed with Athena[49] by first aligning the reference spectra for all data sets and then adjusting the normalization parameters so as to have all spectra match before the edge and approximately 150 eV above the edge.

2.3. Electrochemical Properties. *2.3.1. Preparation of Catalyst Ink and MEAs.* To prepare the catalyst ink, 0.3 g of catalyst was taken in a glass vial, and deionized water was added dropwise to blanket the catalyst surface. Six milliliters of methanol and 5 wt % Nafion 1100 (loading of 30% with respect to total catalyst weight) were added. Methanol was found to be a good dispersing agent for the catalysts. However, to prevent any reactions with the catalyst and air, drops of water were first added to completely wet the catalyst prior to methanol addition. This Nafion loading translated to an ionomer/catalyst weight ratio of 0.43/1. The resultant dispersion was sonicated for 1 h to obtain the catalyst ink. To prepare the MEA, a Nafion 211 membrane was cut into a square, 3.5 cm by 3.5 cm, and the catalyst ink was sprayed on the either side of the membrane using a spray gun, under flowing nitrogen gas. The spraying was

done intermittently (i.e., layer by layer) to prevent any damage to the membrane. To ensure controlled and uniform drying, a heating lamp was placed behind the membrane during the spraying process. The electrocatalyst loading was determined gravimetrically. The anode loading was maintained at 0.2 mg_{Pt} cm^{-2} and the cathode loading was kept at 0.4 mg_{Pt} cm^{-2}. For all MEAs, the anodes were prepared with commercially sourced 46% Pt/C TKK catalysts, whereas the cathodes were made with 20% Pt/$Ta_{0.3}Ti_{0.7}O_2$, 20% Pt/C, or 46% Pt/C. After the desired loading was obtained, two 5 cm^2 pieces of gas diffusion layer (GDL; SGL carbon 10 BB) were used to sandwich the catalyst-coated membrane. The entire assembly was then hot-pressed at 120 °C for 1 min at 7 MPa. The resultant MEAs were used for fuel cell testing.

2.3.2. MEA Performance. Polarization curves were obtained using a Compact Fuel Cell Test System, model 850C (Scribner Associates, Inc.). Before testing for fuel cell polarization, linear sweep voltammetry (LSV) and cyclic voltammetry (CV) experiments were performed, and cell conditioning was carried out. LSV was performed by passing H_2 on the anode at 200 cc/min and N_2 on the cathode at 200 cc/min and measuring the hydrogen crossover current while scanning the working electrode (cathode) potential from 0.05 to 0.8 V vs the anode pseudoreference electrode at a scan rate of 4 mV/s. This was done to ensure MEA integrity was not compromised as a result of either excessive hydrogen crossover or internal short circuits or both. The CV experiment was performed by passing H_2 on the anode at 200 cc/min and N_2 on the cathode at 200 cc/min and measuring the current while scanning the working electrode (cathode) potential from 0.05 to 0.8 V, back to 0.05, vs the anode pseudoreference at a scan rate of 20 mV/s. Before measuring the CV, the cathode was subjected to potential cycling at 100 mV/s from 0 to 1.2 V at least 10 times to standardize the electrode surface. The electrochemically active surface area (ECSA) was estimated using the hydrogen desorption peak on the CV measured at 80 °C. The method is provided in the Supporting Information (SI).[32]

Fuel cell polarization experiments were performed after conditioning the MEA by holding the cell at a constant voltage of 0.55 V for 90 min, followed by running current scans repeatedly until convergence to ensure stable operation at 80 °C and 75% relative humidity (RH; corresponding to a saturator dew point of 73 °C). Fuel/oxidant stoichiometric ratios of 2, with minimum flows of 0.2 SLPM at each electrode, were employed during testing. Subsequently, after stabilization, MEA polarization was recorded under these conditions with hydrogen as the fuel and oxygen, air, 21% oxygen (balance helium), and 4% oxygen (balance nitrogen) as oxidants. The current was scanned from zero (corresponding to open circuit) to a value where the cell voltage dropped below 0.3 V, with each current held for 4 min; an average of 8−10 measurements were recorded at each current value. At the end of all polarization experiments (with all oxidants) for a given MEA, LSV and CV experiments were performed again to ensure that the MEA had remained intact during performance testing and had not degraded in any way during the performance test. Three repeat measurements were performed for each type of MEA.

2.3.3. Evaluation of Catalyst Stability Using Accelerated Stability Test (AST) Protocols. The AST protocol[20b,50] employed in this study to study support stability (hereinafter termed start−stop protocol) was as follows: The working electrode (cathode) potential was cycled in a triangular waveform between 1.0 and 1.5 V vs RHE at a scan rate of 500 mV/s for 10 000 cycles (see SI Figure S2). This protocol aggressively simulated the startup−shutdown transients in an operating PEFC. A second AST protocol (termed load cycling protocol) was used to investigate the degradation/dissolution of the platinum catalyst. The protocol involved cycling the cathode potential in a rectangular waveform from 0.6 to 0.95 V vs RHE for 10 000 cycles and mimicked no-load to full-load transitions during fuel cell operation (see ESI Figure S2). Both of these tests were performed in H_2/N_2 mode (at the anode and cathode, respectively) at 80 °C and 75% RH. After 10 000 cycles, MEA polarization data was again obtained using hydrogen as the fuel and oxygen, air, 21% oxygen (balance helium), and 4% oxygen (balance nitrogen) as oxidants, as described earlier, to investigate the influence of support, catalyst degradation, or both on performance. Post-mortem TEM studies were performed to identify changes in the catalyst/support microstructure after exposure to these ASTs. The MEAs were disassembled, and the catalyst was recovered from the electrode using a diamond-tipped tool after wetting the electrode with a few drops of isopropyl alcohol. Samples were taken from various locations along the electrode.

3. RESULTS AND DISCUSSION

3.1. Microstructure. The microstructure of the Ta-modified TiO_2 supports and derivative catalysts as elucidated by the X-ray diffraction and TEM has been described earlier.[32] Briefly, Ta was found to be completely incorporated into the $Ta_{0.3}Ti_{0.7}O_2$ structure (no peaks from TaO_2 or Ta_2O_5 were observed). $Ta_{0.3}Ti_{0.7}O_2$ particles ranged in size from 70 to 85 nm, had a BET surface area of 26 m^2/g, and had an electron conductivity of 0.2 S/cm. The electron conductivity was measured using a technique we have described in prior work.[32] The details are reproduced in the SI. Pt particle sizes in 20% Pt/$Ta_{0.3}Ti_{0.7}O_2$ and 20% Pt/C catalysts were found to be 4.4 (±0.4) nm and 4.1(±0.6) nm, respectively; the similarity in sizes was deliberate and induced by the identical Pt synthesis procedure followed, with the intent of comparing catalyst samples with similar surface free energies. The 46% Pt/C catalyst had an average Pt particle size of 3.0 (±0.2) nm.

The Pt L3-edge X-ray absorption near edge spectroscopy (XANES) region of the 20% Pt/$Ta_{0.3}Ti_{0.7}O_2$ catalyst has been plotted and compared with 20% and 46% Pt/C (see Figure 1).

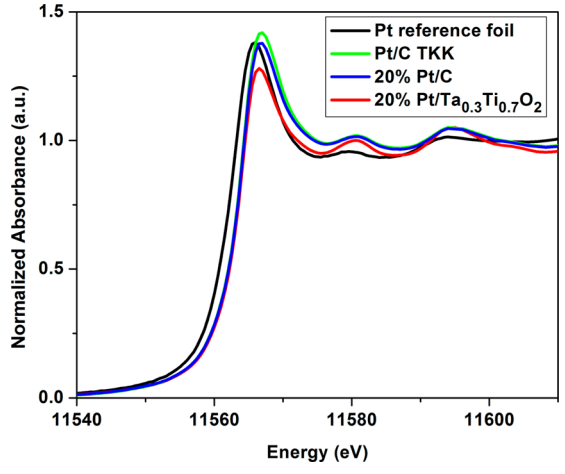

Figure 1. Pt L3-edge XANES spectra of 20% Pt/$Ta_{0.3}Ti_{0.7}O_2$, 46% Pt/C, 20% Pt/C catalysts, and Pt foil.

dx.doi.org/10.1021/cs500116h | ACS Catal. 2014, 4, 1516−1525

The Pt L2-edge XANES regions of the 20% Pt/$Ta_{0.3}Ti_{0.7}O_2$, 20% Pt/C, and 46% Pt/C are shown in SI Figure S3.The area under the white line curve, the magnitude of which is a direct measure of d band vacancies, was in the order 46% Pt/C ~ Pt foil ~ 20% Pt/C > 20% Pt/$Ta_{0.3}Ti_{0.7}O_2$, with the 20% Pt/$Ta_{0.3}Ti_{0.7}O_2$ showing the lowest area under the white line curve, that is, exhibiting the greatest shift of electron density from the support to Pt. The large decrease in its white line intensity, and concomitantly the area under the curve, was attributed to SMSI,[51] between Pt and the $Ta_{0.3}Ti_{0.7}O_2$ support. This mechanism explains the facile nature of electron donation from the $Ta_{0.3}Ti_{0.7}O_2$ support to Pt metal, leading ultimately to a drastic decrease in the d band vacancy of Pt, as reflected in the results of the calculation to determine the number of unfilled d states (h_{Ts}).

The 20% Pt/$Ta_{0.3}Ti_{0.7}O_2$ catalyst had the lowest number of unfilled d states (h_{Ts} = 1.47) compared with all the other samples, namely, Pt foil (1.60), 20% Pt/C (1.59), and 46% Pt/C (1.61), as shown in Figure 2. XPS data, shown previously[32]

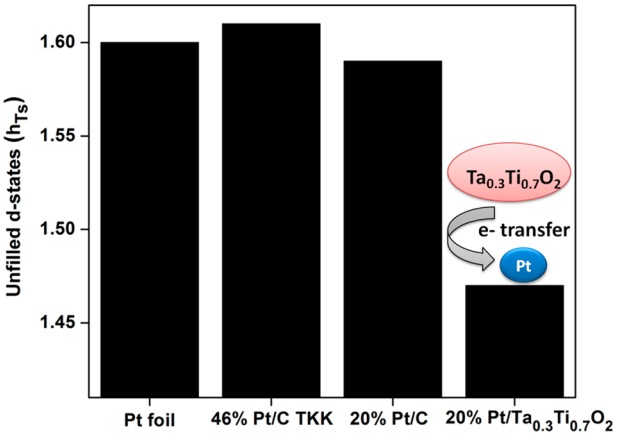

Figure 2. Variation in unfilled d states for 20% Pt/$Ta_{0.3}Ti_{0.7}O_2$, 46% Pt/C, 20% Pt/C catalysts, and Pt foil.

and reproduced in SI Figure S4, also revealed that the Pt 4f signal for Pt deposited on $Ta_{0.3}Ti_{0.7}O_2$ was observed at a binding energy (BE) of 71.20 eV, which was ~600 meV lower when compared with the corresponding signal for Pt deposited on carbon (71.73 eV). This difference in the Pt 4f BE was attributed to a local increase in the electron density at the Pt site when it was deposited on $Ta_{0.3}Ti_{0.7}O_2$ and corroborated that SMSI existed in 20% Pt/$Ta_{0.3}Ti_{0.7}O_2$. A similar decrease in the Pt 4f BE has also been reported for Pt deposited on other oxides of titanium.[51b,52] These results unequivocally confirmed that the SMSI between $Ta_{0.3}Ti_{0.7}O_2$ and Pt resulted in facile electron donation from the $Ta_{0.3}Ti_{0.7}O_2$ support to Pt metal. Variations in the adsorption strength of oxygen and/or oxygen intermediates (formed during ORR) on the surface of Pt due to the SMSI-derived modification in the electronic structure of Pt can lead to improvement in electrocatalytic activity.[44,45,53] Therefore, unlike carbon, $Ta_{0.3}Ti_{0.7}O_2$ can play an important role as cocatalyst for Pt for the ORR.

3.2. Electrochemical Properties. *3.2.1. Fuel Cell Performance.* The beginning of life (BoL) H_2–air polarization curves for the different MEAs, shown in Figure 3, clearly indicate that 20% Pt/$Ta_{0.3}Ti_{0.7}O_2$ has very promising performance in an operating fuel cell comparable to and even exceeding performance obtained using other noncarbon support materi-

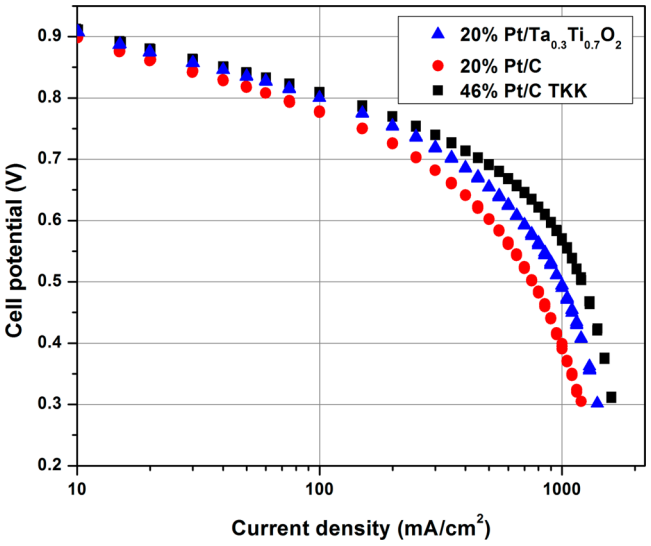

Figure 3. H_2–air fuel cell performance of MEAs prepared using 46% Pt/C at the anode (loading = 0.2 mg_{Pt} cm^{-2}) and 20% Pt/$Ta_{0.3}Ti_{0.7}O_2$, 20% Pt/C, and 46% Pt/C (loading =0.4 mg_{Pt} cm^{-2}) at the cathode at 80 °C and 75% RH.

als[22a,34] under similar operating environments. The polarization data obtained on each type of MEA with the four different oxidants are shown in th eSI, Figures S5–S7. This polarization data obtained was analyzed following the method initially proposed by Williams et al. and is found in the literature.[19c,20b,54] The objective of this analysis was to quantitatively estimate key ohmic, mass transport, and kinetic parameters as well as the distribution of overpotentials in the MEAs prepared using the various electrocatalysts studied. In implementing the methods described, four main sources of polarization losses were estimated: (1) nonelectrode ohmic overpotential ($\eta_{ohmic,nonelectrode}$, due to ohmic losses in the electrolyte membrane and any contact resistances), (2) electrode ohmic overpotential ($\eta_{ohmic,electrode}$, due to ohmic losses in the electrode), (3) nonelectrode concentration overpotential ($\eta_{conc,nonelectrode}$, due to mass transport losses in the GDL and through binder film in the electrode where oxygen is not consumed), and (4) electrode concentration overpotential ($\eta_{conc,electrode}$, arising from mass transport losses due to combined reaction and diffusion within the electrode where oxygen is consumed).

Ohmic Losses. Table 1 reports the overpotential at 1000 mA/cm^2, with air as oxidant, for each MEA tested. Given that all MEAs had the same membrane, there should have been no variation in membrane resistance. The observed values suggested that the contact resistances at the membrane electrode interface were similar for all three electrocatalysts.

Table 1. Distribution of Overpotential: H_2/Air Operation at 80 °C and 75% RH at a Current Density of 1000 mA/cm^2

overpotential (mV)	20% Pt/$Ta_{0.3}Ti_{0.7}O_2$ i = 1000 mA/cm^2	20% Pt/C i = 1000 mA/cm^2	46% Pt/C i = 1000 mA/cm^2
$\eta_{ohmic,nonelectrode}$	61 ± 2	59 ± 3	59 ± 4
$\eta_{ohmic,electrode}$	49 ± 2	36 ± 3	31 ± 1
$\eta_{conc,nonelectrode}$	144 ± 5	125 ± 5	64 ± 4
$\eta_{conc,electrode}$	33 ± 2	28 ± 2	31 ± 3

dx.doi.org/10.1021/cs500116h | ACS Catal. 2014, 4, 1516–1525

Table 2. Characteristic Parameters for MEAs Tested at 80 °C, 75% RH and Ambient Pressure[a]

parameter/metric	20% Pt/$Ta_{0.3}Ti_{0.7}O_2$	20% Pt/C	46% Pt/C
b (mV/dec)	70 ± 2	74 ± 2	68 ± 2
i_0 (mA/cm^2)	(6.8 ± 0.3) × 10^{-3}	(2.1 ± 0.2) × 10^{-3}	(10.2 ± 0.2) × 10^{-3}
j_m (mA mg$^{-1}{}_{Pt}$) @ 0.9 V	185 ± 2	148 ± 3	224 ± 6[b]
js (μA cm$^{-2}{}_{Pt}$) @ 0.9 V	219 ± 3	196 ± 2	241 ± 3
ECSA (m^2/g_{Pt})[c]	60 ± 2	57 ± 1	65 ± 2
nonelectrode ohmic resistance (mΩ cm^2)	61 ± 3	59 ± 1	59 ± 2
electrode ohmic resistance (mΩ cm^2)	45 ± 2	33 ± 2	30 ± 3
limiting current, air (mA cm^2)	1605 ± 64	1540 ± 62	1680 ± 54
Post AST (start stop cycling)			
j_m (mA mg$^{-1}{}_{Pt}$) @ 0.9 V	174 ± 3		
Post AST (load cycling)			
j_m (mA mg$^{-1}{}_{Pt}$) @ 0.9 V	184 ± 3	146 ± 3	224 ± 4

[a]2 times stoichiometric flow rate of reactants. Anode catalyst loading, 0.2 mg/cm^2; cathode catalyst loading, 0.4 mg/cm^2. [b]Consistent with typical mass activity values for 46% Pt/C reported in the literature, ~200 mA/mg_{Pt}.[38,40] [c]In a PEFC, the OCV of Pt/TiO_2 was found to be as low as 0.75 V vs RHE, whereas the ECSA was found to be lower than 5 m^2/g_{Pt}.

The effective "electrolyte + contact" resistances are reported in Table 2.

The ohmic resistance in the electrode, R_e, was estimated using the data corrected for $\eta_{ohmic,nonelectrode}$. The calculated R_e values for MEAs prepared using Pt/$Ta_{0.3}Ti_{0.7}O_2$, 20% Pt/C, and 46% Pt/C were 45, 33, and 30 mΩ cm^2, respectively (Table 2). The values obtained for the Pt/C-based electrodes were in line with expectations and were largely attributed to the resistance to proton transport in the electrode layer. The higher R_e for 20% Pt/$Ta_{0.3}Ti_{0.7}O_2$ compared with Pt/C-based electrodes was attributed to the fact that electron conduction through the $Ta_{0.3}Ti_{0.7}O_2$ support was inhibited somewhat by the higher proportion of ionomer in this electrode, as discussed below.

Mass Transport Losses. The $\eta_{conc,nonelectrode}$ was larger for the MEAs prepared with 20 wt % Pt loadings, and the electrode concentration overpotential ($\eta_{conc,electrode}$) was almost identical for all MEAs. In the case of 20% Pt/C, the electrode thickness was higher because the Pt loading on the cathode was maintained consistent for all catalysts. This contributed to the larger mass transport losses. For 20% Pt/$Ta_{0.3}Ti_{0.7}O_2$, although the electrode layer thickness was about the same as that of 46% Pt/C (due to the denser support), the proportion of ionomer to support was higher. The 20% Pt/$Ta_{0.3}Ti_{0.7}O_2$-based MEA therefore had a thicker ionomer layer covering the Pt surface and, hence, was more prone to condensed phase transport limitations (transport of oxygen through this film to reach active catalyst surface), leading to a larger $\eta_{conc,nonelectrode}$. Among the three different electrocatalysts, the magnitudes of this overpotential were consistent with the limiting current densities that were estimated.

The helox–air gain was plotted against the O_2–air gain for each current density (Figure 4) to identify whether O_2 transport within the various electrodes studied was hindered by gas phase or condensed phase diffusion limitations (or by both).[54a] All the MEAs primarily exhibited gas phase transport limitations. The 20% Pt/$Ta_{0.3}Ti_{0.7}O_2$, however, showed a greater tendency toward condensed phase transport limitations (smaller slope of the gain plot), which related well to the magnitude of nonreacting transport and electrode ohmic losses estimated from polarization data analysis (attributed to a thicker ionomer film in the electrode).

Activation Losses. Subsequent to these corrections, low current density data (10–100 mA/cm^2) was used to calculate

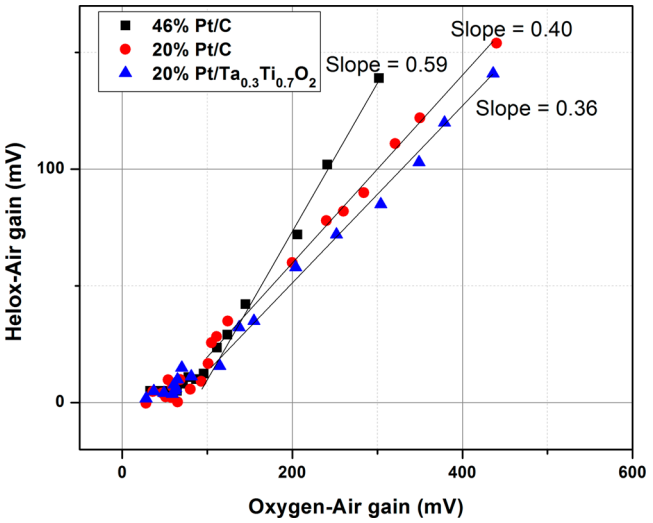

Figure 4. Helox–air gain vs O_2–air gain of MEAs prepared with 46% Pt/C, 20% Pt/C, and 20% Pt/$Ta_{0.3}Ti_{0.7}O_2$ at 80 °C and 75% RH.

the Tafel slope (Figure 5). The Tafel slopes for all catalysts were similar (70 ± 2, 74 ± 2, and 68 ± 2 mV/decade for 20% Pt/C and 20% Pt/$Ta_{0.3}Ti_{0.7}O_2$, respectively), suggesting similar ORR mechanisms were at play and that the support did not unduly influence the reaction mechanism.

46% Pt/C was the most active among the 3 catalysts and exhibited higher ECSA, exchange current density, and mass activity (Table 2) than the other catalysts. This was quite in line with expectations, given that this catalyst had a much smaller Pt particle size. The trends in mass activity values were consistent for the catalysts across the RDE[32] and MEA techniques. In both methods studied, Pt/$Ta_{0.3}Ti_{0.7}O_2$ was found to have a lower mass activity than Pt/C TKK.

When comparing across samples with similar Pt particle sizes, 20% Pt/$Ta_{0.3}Ti_{0.7}O_2$ exhibited a higher ECSA, exchange current density, and mass activity than 20% Pt/C (Table 2), although the 20% Pt/$Ta_{0.3}Ti_{0.7}O_2$ catalyst had an average Pt particle size that was slightly greater than 20% Pt/C. Although this trend seemed anomalous at first sight, it could be rationalized. As demonstrated earlier using XANES analysis, the $Ta_{0.3}Ti_{0.7}O_2$ support donated electrons to the Pt catalyst, thereby decreasing its d band vacancy through SMSI. These interactions altered the adsorption strength of oxygen molecules on the Pt surface

dx.doi.org/10.1021/cs500116h | ACS Catal. 2014, 4, 1516–1525

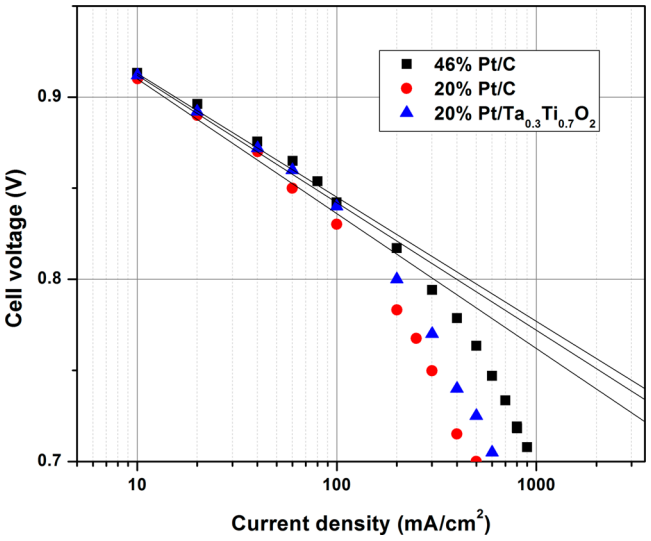

Figure 5. Analysis of H_2/O_2 polarization data for MEAs with 46% Pt/C, 20% Pt/C, and 20% Pt/$Ta_{0.3}Ti_{0.7}O_2$. The straight lines correspond to data corrected for ohmic (membrane + cathode) and nonreacting O_2 transport losses.

favorably, resulting in enhanced catalytic activity. Other candidate mechanisms contributing to increased fuel cell performance include adlineation (proposed by Fleischmann et al.[55]) or the formation of an interface between the support and catalyst and enhanced diffusion of intermediates to the surface, as described by the spillover model proposed by Boudart et al.[56] Although no evidence of any SMSI was observed (from XANES data) in 46% Pt/C, the fact that it possessed the highest activity among the catalysts studied was not an anomaly and could be attributed to the lower Pt particle size in this material.

3.2.2. Electrochemical Stability of 20% Pt/$Ta_{0.3}Ti_{0.7}O_2$ in a PEFC. Start–Stop cycling: Figure 6 represents the polarization curves of the MEAs prepared by 46% Pt/C, 20% Pt/C, and

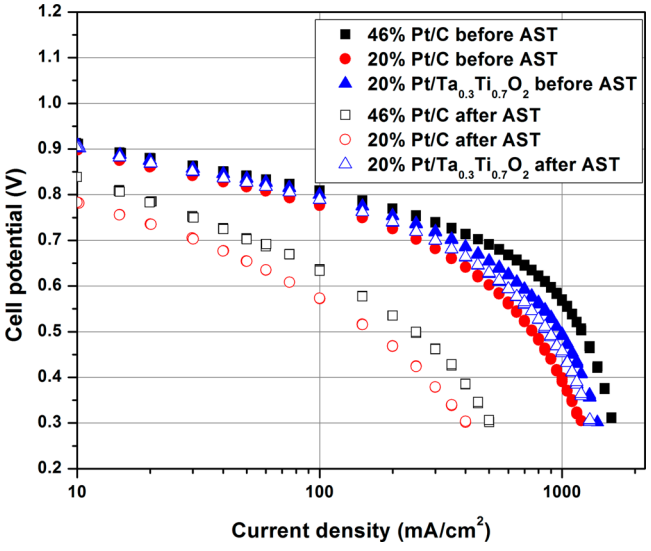

Figure 6. H_2–air fuel cell performance of MEAs prepared using 46% Pt/C at the anode (loading = 0.2 mg_{Pt} cm^{-2}) and 46% Pt/C, 20% Pt/C, and 20% Pt/$Ta_{0.3}Ti_{0.7}O_2$ (loading = 0.4 mg_{Pt} cm^{-2}) at the cathode at 80 °C and 75% RH before and after the AST using the start–stop protocol.

20% Pt/$Ta_{0.3}Ti_{0.7}O_2$ electrocatalysts in a single cell before and after this AST. The effects of start–stop cycling on cell performance were negligible in the case of the 20% Pt/$Ta_{0.3}Ti_{0.7}O_2$ electrocatalyst; a slight decrease in cell voltage (~23 mV) at 0.4 Acm^{-2} was observed after 10 000 AST cycles. However, the MEAs prepared with 46% and 20% Pt/C catalysts exhibited a large voltage drop (~330 and 340 mV, respectively, at 0.4 Acm^{-2}) after 10 000 AST cycles; this was patently due to carbon corrosion and subsequent detachment and agglomeration of catalyst particles.[22c] The changes in mass activity for each catalyst as a result of the AST are shown in Table 2 and reinforce the claim to high stability of the 20% Pt/$Ta_{0.3}Ti_{0.7}O_2$ electrocatalyst. The electrochemical corrosion of the carbon surface led to changes in the surface chemistry of the carbon and an increase in the hydrophilicity of the catalyst layer and the GDL, which negatively affected the transport of the reactant gas.[22b] Carbon corrosion also results in thinning of the electrode layer, leading to a reduction in the electrical contact with the GDL. All these factors lead to a significant decrease in fuel cell performance.

To examine the influence of start–stop potential cycling on the structure of the 20% Pt/$Ta_{0.3}Ti_{0.7}O_2$ catalyst, samples from the tested MEA were analyzed by TEM. Figure 7 shows TEM images of the catalyst particles of 20% Pt/$Ta_{0.3}Ti_{0.7}O_2$, 20% Pt/C, and 46% Pt/C before and after 10 000 cycles of the start–

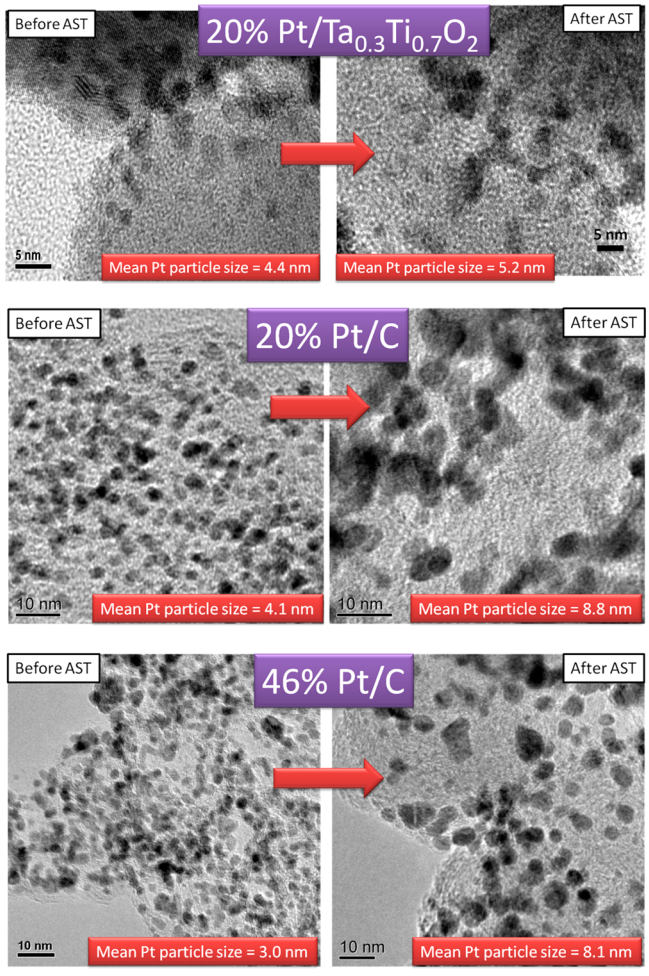

Figure 7. TEM images of 20% Pt/$Ta_{0.3}Ti_{0.7}O_2$, 20% Pt/C and 46% Pt/C particles before and after the AST using the start–stop protocol.

dx.doi.org/10.1021/cs500116h | ACS Catal. 2014, 4, 1516–1525

stop AST. Extensive growth of Pt particles was observed for 46% and 20% Pt/C, which is consistent with literature reports.[3a,57] Moreover, irregularly shaped particles were observed after the AST. The degradation mechanism of Pt/C catalysts during potential cycling occurs via Pt dissolution and redeposition (growth via Ostwald ripening); coalescence, via crystal migration; and detachment of Pt particles, from the carbon support.[3a] Carbon corrosion promotes particle coalescence via crystal migration, which likely leads to the formation of such irregularly shaped Pt particles. In contrast, although samples from more than 10 points within the electrode were exhaustively examined, no significant differences between the pristine and cycled 20% Pt/$Ta_{0.3}Ti_{0.7}O_2$ catalysts were observed. The shapes of the Pt particles in post-test 20% Pt/$Ta_{0.3}Ti_{0.7}O_2$ samples were almost identical to those in pristine samples. Strong interactions between Pt particles and the oxide support and the inherent superior support stability at high potentials account for this exceptional stability of 20% Pt/$Ta_{0.3}Ti_{0.7}O_2$. This high stability is consistent with predictions based on the XANES results. The XANES results, which showed the existence of SMSI between Pt and $Ta_{0.3}Ti_{0.7}O_2$, could also be used to explain the higher stability of the 20% Pt/$Ta_{0.3}Ti_{0.7}O_2$ electrocatalysts during start–stop cycling because the SMSI observed facilitated strong Pt attachment to the support, thereby leading to enhanced overall catalyst stability.

Load Cycling. Figure 8 shows the performance of the MEAs prepared by the 20% Pt/$Ta_{0.3}Ti_{0.7}O_2$, 20% Pt/C, and 46% Pt/C catalysts before and after 10 000 cycles of the load cycling AST. None of the catalysts showed significant deterioration in performance. Although each of these catalysts showed a large decrease in ECSA upon load cycling, the fuel cell performance of the catalysts was not significantly impacted. The ECSA of 20% Pt/$Ta_{0.3}Ti_{0.7}O_2$, 20% Pt/C, and 46% Pt/C decreased by 35%, 44%, and 47%, respectively. This confirmed that platinum dissolution did occur on all the supports when they were subjected to load cycling.

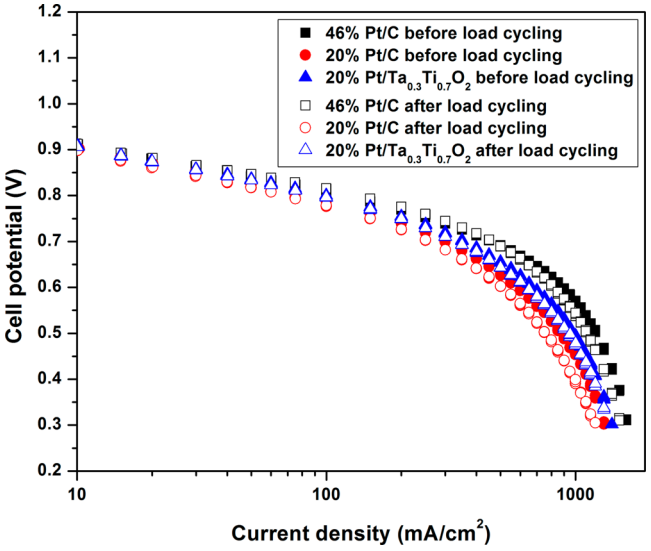

Figure 8. H_2–air fuel cell performance of MEAs prepared using 46% Pt/C at the anode (loading = 0.2 mg_{Pt} cm^{-2}) and 46% Pt/C, 20% Pt/C, and 20% Pt/$Ta_{0.3}Ti_{0.7}O_2$ (loading = 0.4 mg_{Pt} cm^{-2}) at the cathode at 80 °C and 75% RH before and after AST using load cycling protocol.

Figure 9 shows the TEM images of the catalyst particles of 20% Pt/$Ta_{0.3}Ti_{0.7}O_2$, 20% Pt/C, and 46% Pt/C before and after

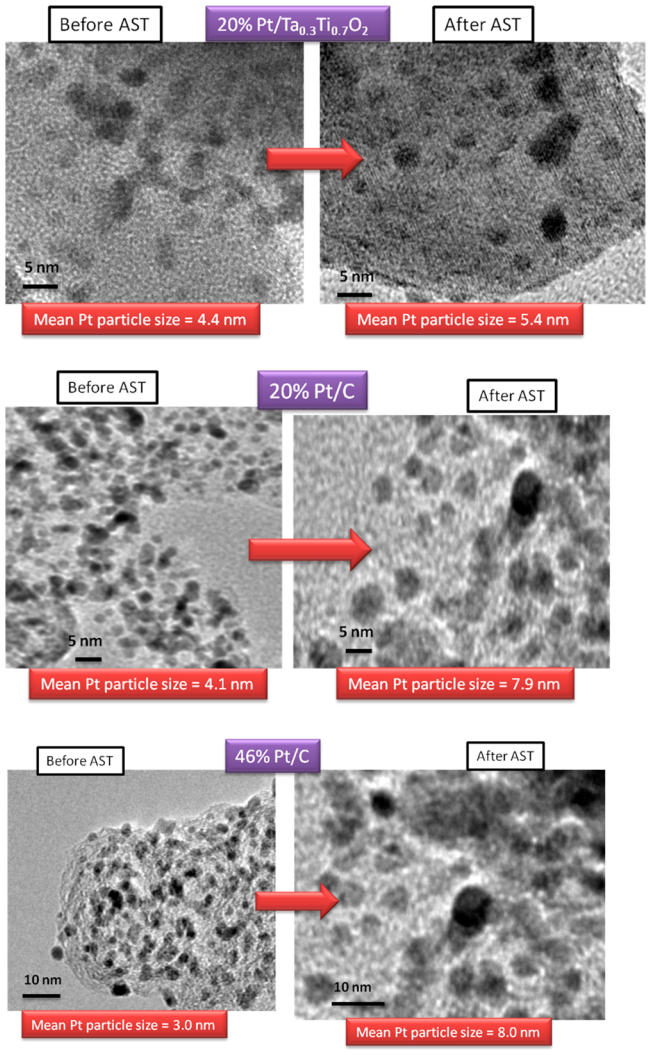

Figure 9. TEM images of 20% Pt/$Ta_{0.3}Ti_{0.7}O_2$, 20% Pt/C and 46% Pt/C particles before and after the AST using the load cycling protocol.

10 000 cycles of the load cycling AST. All catalysts showed evidence of Pt particle growth; however, the extent of platinum growth was lower in the case of 20% Pt/$Ta_{0.3}Ti_{0.7}O_2$ when compared with 20% Pt/C and 46% Pt/C. Although the higher platinum dissolution/agglomoration rate of 46% Pt/C could be attributed to the higher initial surface free energy of the smaller Pt nanoparticles, the fact that the 20% Pt/$Ta_{0.3}Ti_{0.7}O_2$ exhibited less platinum dissolution under identical conditions than 20% Pt/C further reinforced the presence of SMSI that stabilized the platinum particles. Clearly, the synthesis and processing of 20% Pt/$Ta_{0.3}Ti_{0.7}O_2$ can be further optimized to reinforce the SMSI and further stabilize the platinum particles, and this is an ongoing task. At 1 A/cm^2, the loss in voltage of 20% Pt/$Ta_{0.3}Ti_{0.7}O_2$, 20% Pt/C, and 46% Pt/C was ~15, 50, and 30 mV, respectively. The performance losses in 20% Pt/C and 46% Pt/C were negligible compared with the catastrophic losses observed during start–stop cycling. These results demonstrate conclusively that support corrosion is far more severe in terms of consequences on performance than platinum dissolution. Pt dissolution and agglomeration does occur during

dx.doi.org/10.1021/cs500116h | *ACS Catal.* 2014, 4, 1516–1525

load cycling, but its impact on MEA performance by itself is not as acute as the support corrosion phenomenon.

4. CONCLUSIONS

A robust noncarbon $Ta_{0.3}Ti_{0.7}O_2$ support has been synthesized, characterized, catalyzed with platinum, and tested in an operating fuel cell. The 20% $Pt/Ta_{0.3}Ti_{0.7}O_2$ catalyst demonstrates fairly good activity and very high durability in an operating fuel cell when compared against a commercial 46% Pt/C (TKK) benchmark, and a like-for-like 20% Pt/C catalyst synthesized in-house, with a similar platinum particle size and loading. The 20% $Pt/Ta_{0.3}Ti_{0.7}O_2$ catalyst exhibited an initial fuel cell mass activity of 185 mA/mg_{Pt} (at 0.9 V vs RHE) that was higher when compared with that of 20% Pt/C (148 mA/mg_{Pt}). The 20% $Pt/Ta_{0.3}Ti_{0.7}O_2$ catalyst exhibited exceptional electrochemical stability compared with both the carbon supported catalysts and showed a loss of only 23 mV at 0.4 A/cm^2 compared wtih a loss of 330 and 340 mV at the same current density after 10 000 cycles of a simulated start-up/shut down potential cycling AST. This clearly evidenced that the $Ta_{0.3}Ti_{0.7}O_2$ served as a highly corrosion-resistant support. Exposure to load-cycling ASTs revealed that platinum dissolution did occur in all the catalysts, but it was somewhat lower for the 20% $Pt/Ta_{0.3}Ti_{0.7}O_2$ catalyst. Unlike the start–stop AST, exposure to the load cycling AST had minimal impact on performance, confirming that the fuel cell is far more forgiving of platinum dissolution in itself than it is of support corrosion. XANES analysis unequivocally revealed the presence of strong metal/support interactions between Pt particles and $Ta_{0.3}Ti_{0.7}O_2$. These interactions contributed to the higher activity and stability of the 20% $Pt/Ta_{0.3}Ti_{0.7}O_2$ catalyst. Although the initial fuel cell performance of 20% $Pt/Ta_{0.3}Ti_{0.7}O_2$ fell short of the accepted benchmark of 46% Pt/C, this catalyst shows much superior durability by virtue of the highly stable support, suggesting that it is very much a viable material for automotive fuel cell stacks.

■ ASSOCIATED CONTENT

Supporting Information

All chemicals used during synthesis, electron conductivity measurement technique, durability protocols, XANES characterization, XPS results, and fuel cell performance data before and after start–stop cycling. This material is available free of charge via the Internet at http://pubs.acs.org.

■ AUTHOR INFORMATION

Corresponding Author

*Email: ramani@iit.edu.

Notes

The authors declare no competing financial interest.

■ ACKNOWLEDGMENTS

This work was supported by NSF Award No. 0847030. The authors would like to acknowledge Prof. Carlo Segre, Department of Physics, Illinois Institute of Technology for XAS spectra and analyses. Materials Research Collaborative Access Team (MRCAT) operations are supported by the Department of Energy and the MRCAT member institutions. Use of the Advanced Photon Source, an Office of Science User Facility operated for the U.S. Department of Energy (DOE) Office of Science by Argonne National Laboratory, was supported by the U.S. DOE under Contract No. DE-AC02-06CH11357. We would like to acknowledge with gratitude the opportunity to utilize these user facilities.

■ REFERENCES

(1) Borup, R.; Meyers, J.; Pivovar, B.; Kim, Y. S.; Mukundan, R.; Garland, N.; Myers, D.; Wilson, M.; Garzon, F.; Wood, D.; Zelenay, P.; More, K.; Stroh, K.; Zawodzinski, T.; Boncella, J.; McGrath, J. E.; Inaba, M.; Miyatake, K.; Hori, M.; Ota, K.; Ogumi, Z.; Miyata, S.; Nishikata, A.; Siroma, Z.; Uchimoto, Y.; Yasuda, K.; Kimijima, K.-i.; Iwashita, N. *Chem. Rev.* **2007**, *107* (10), 3904–3951.

(2) (a) Collier, A.; Wang, H. J.; Yuan, X. Z.; Zhang, J. J.; Wilkinson, D. P. *Int. J. Hydrogen Energy* **2006**, *31* (13), 1838–1854. (b) Stevens, D. A.; Hicks, M. T.; Haugen, G. M.; Dahn, J. R. *J. Electrochem. Soc.* **2005**, *152* (12), A2309–A2315. (c) Davies, D. P.; Adcock, P. L.; Turpin, M.; Rowen, S. J. *J. Appl. Electrochem.* **1999**, *30* (1), 101–105.

(3) (a) Shao-Horn, Y.; Sheng, W. C.; Chen, S.; Ferreira, P. J.; Holby, E. F.; Morgan, D. *Top. Catal.* **2007**, *46*, 285. (b) Ferreira, P. J.; la O, G. J.; Shao-Horn, Y.; Morgan, D.; Makharia, R.; Kocha, S.; Gasteiger, H. A. *J. Electrochem. Soc.* **2005**, *152*, A2256.

(4) Kinoshita, K. Wiley: New York, 1988; p 316.

(5) (a) Takeuchi, N.; Fuller, T. F. *J. Electrochem. Soc.* **2008**, *155* (7), B770–B775. (b) Reiser, C. A.; Bregoli, L.; Patterson, T. W.; Yi, J. S.; Yang, J. D.; Perry, M. L.; Jarvi, T. D. *Electrochem. Solid-State Lett.* **2005**, *8* (6), A273–A276.

(6) (a) Patterson, T. W.; Darling, R. M. *Electrochem. Solid-State Lett.* **2006**, *9*, A183. (b) Roen, L. M.; Paik, C. H.; Jarvi, T. D. *Electrochem. Solid-State Lett.* **2004**, *7*, A19. (c) Kangasniemi, K. H.; Condit, D. A.; Jarvi, T. D. *J. Electrochem. Soc.* **2004**, *151*, E125. (d) Meyers, J. P.; Darling, R. M. *J. Electrochem. Soc.* **2006**, *153*, A1432.

(7) Stevens, D. A.; Dahn, J. R. *Carbon* **2005**, *43* (1), 179–188.

(8) (a) Antolini, E. *Appl. Catal., B* **2009**, *88*, 1–24. (b) Zhou, J.; Zhou, X.; Sun, X.; Li, R.; Murphy, M.; Ding, Z.; Sun, X.; Sham, T.-K. *Chem. Phys. Lett.* **2007**, *437* (4–6), 229–232.

(9) Wang, Y.-J.; Wilkinson, D. P.; Zhang, J. *Chem. Rev.* **2011**, *111* (12), 7625–7651.

(10) Qi, Z. *Chem. Commun.* **1998**, *1*, 15–16.

(11) (a) Kou, R.; Shao, Y.; Mei, D.; Nie, Z.; Wang, D.; Wang, C.; Viswanathan, V. V.; Park, S.; Aksay, I. A.; Lin, Y.; Wang, Y.; Liu, J. *J. Am. Chem. Soc.* **2011**, *133*, 2541–2547. (b) Banis, M. N.; Sun, S.; Meng, X.; Zhang, Y.; Wang, Z.; Li, R.; Cai, M.; Sham, T.-K.; Sun, X. *J. Phys. Chem. C* **2013**, *117* (30), 15457–15467. (c) Saha, M. S.; Li, R.; Cai, M.; Sun, X. *J. Power Sources* **2008**, *185* (2), 1079–1085.

(12) (a) Evans, S. A. G.; Terry, J. G.; Plank, N.; Walton, A.; Keane, L.; Campbell, C.; Ghazal, P.; Beattie, J.; Su, T.; Crain, J.; Mount, A. *Electrochem. Commun.* **2005**, *7*, 125. (b) Musthafa, O. T. M.; Sampath, S. *Chem. Commun.* **2008**, *1*, 67–69. (c) Avasarala, B.; Haldar, P. *Electrochim. Acta* **2010**, *55* (28), 9024–9034.

(13) Sharma, S.; Pollet, B. G. *J. Power Sources* **2012**, *208* (0), 96–119.

(14) (a) Liu, N.; Kourtakis, K.; Figueroa, J. C.; Chen, J. G. *J. Catal.* **2003**, *215*, 254. (b) Chhina, H.; Campbell, S.; Kesler, O. *J. Power Sources* **2007**, *164*, 431. (c) Zellner, M. B.; Chen, J. G. *Catal. Today* **2005**, *99*, 299.

(15) (a) Ganesan, R.; Ham, D. J.; Lee, J. S. *Electrochem. Commun.* **2007**, *9*, 2576. (b) Hara, Y.; Minami, N.; Itagaki, H. *Appl. Catal., A* **2007**, *323*, 86. (c) Hara, Y.; Minami, N.; Matsumoto, H.; Itagaki, H. *Appl. Catal., A* **2007**, *332*, 289.

(16) (a) Santos, A. L.; Profeti, D.; Olivi, P. *Electrochim. Acta* **2005**, *50*, 2615. (b) Sudan Saha, M.; Li, R.; Cai, M.; Sun, X. *Electrochem. Solid-State Lett.* **2007**, *10* (8), B130–B133.

(17) Chhina, H.; Campbell, S.; Kesler, O. *J. Power Sources* **2006**, *161*, 893–900.

(18) (a) Cui, X.; Shi, J.; Chen, H.; Zhang, L.; Guo, L.; Gao, J.; Li, J. *J. Phys. Chem. B* **2008**, *112*, 12024. (b) Rajeswari, J.; Viswanathan, B.; Varadarajan, T. K. *Mater. Chem. Phys.* **2007**, *106*, 168. (c) Saha, M. S.; Banis, M. N.; Zhang, Y.; Li, R.; Sun, X.; Cai, M.; Wagner, F. T. *J. Power Sources* **2009**, *192*, 330–335.

(19) (a) Haas, O. E.; Briskeby, S. T.; Kongstein, O. E.; Tsypkin, M.; Tunold, R.; Børresen, B. T. *J. New Mater. Electrochem. Syst.* **2008**, *11*, 9. (b) Chen, G.; Bare, S. R.; Mallouk, T. E. *J. Electrochem. Soc.* **2003**, *149*,

A1092. (c) Lo, C.-P.; Wang, G.; Kumar, A.; Ramani, V. *Appl. Catal., B* **2013**, *140−141*, 133−140. (d) Lo, C.-P.; Kumar, A.; Ramani, V. *ECS Trans.* **2010**, *33* (1), 493−505.
(20) (a) Chen, Z.; Qiu, Z.; Lu, B.; Zhang, S.; Zhu, W.; Chen, L. *Electrochem. Commun.* **2005**, *7*, 593. (b) Kumar, A.; Ramani, V. K. *Appl. Catal., B* **2013**, *138−139* (0), 43−50. (c) Lo, C.-P.; Ramani, V. *ACS Appl. Mater. Interfaces* **2012**, *4* (11), 6109−6116.
(21) Seger, B.; Kongkanand, A.; Vinodgopal, K.; Kamat, P. V. *J. Electroanal. Chem.* **2008**, *621*, 198−204.
(22) (a) Huang, S. Y.; Ganesan, P.; Park, S.; Popov, B. N. *J. Am. Chem. Soc.* **2009**, *131*, 13898. (b) Huang, S.-Y.; Ganesan, P.; Popov, B. N. *Appl. Catal., B* **2010**, *96* (1−2), 224−231. (c) Ioroi, T.; Akita, T.; Yamazaki, S.-i.; Siroma, Z.; Fujiwara, N.; Yasuda, K. *J. Electrochem. Soc.* **2011**, *158*, C329−C334. (d) Wang, Y.-J.; Wilkinson, D. P.; Zhang, J. *Dalton Trans.* **2012**, *41* (4), 1187−1194. (e) Subban, C. V.; Zhou, Q.; Hu, A.; Moylan, T. E.; Wagner, F. T.; DiSalvo, F. J. *J. Am. Chem. Soc.* **2010**, *132* (49), 17531−17536.
(23) Leroux, F.; Dewar, P. J.; Intissar, M.; Ouvrard, G.; Nazar, L. F. *J. Mater. Chem.* **2002**, *12* (11), 3245−3253.
(24) von Kraemer, S.; Wikander, K.; Lindbergh, G.; Lundblad, A.; Palmqvist, A. E. C. *J. Power Sources* **2008**, *180* (1), 185−190.
(25) Gratzel, M. *Nature (London)* **2001**, *414* (6861), 338−344.
(26) Fujishima, A.; Honda, K. *Nature* **1972**, *238*, 37−38.
(27) (a) Ioroi, T.; Siroma, Z.; Fujiwara, N.; Yamazaki, S.; Yasuda, K. *Electrochem. Commun.* **2005**, *7*, 183. (b) Kolbrecka, K.; Przylski, J. *Electrochim. Acta* **1994**, *39*, 1591.
(28) Goswami, P.; Ganguli, J. N. *Dalton Trans.* **2013**, *42* (40), 14480−14490.
(29) Li, L.; Yang, W.; Ding, Y.; Zhu, X. *J. Semicond.* **2012**, *33* (1), 012002.
(30) Wenfang, Z.; Qingju, L.; Zhongqi, Z.; Ji, Z. *J. Phys. D: Appl. Phys.* **2010**, *43* (3), 035301.
(31) (a) Chhina, H.; Campbell, S.; Kesler, O. *J. Electrochem. Soc.* **2009**, *156*, B1232−B1237. (b) Liu, Y.; Szeifert, J. M.; Feckl, J. M.; Mandlmeier, B.; Rathousky, J.; Hayden, O.; Fattakhova-Rohlfing, D.; Bein, T. *ACS Nano* **2010**, *4* (9), 5373−5381. (c) Park, K.-W.; Seol, K.-S. *Electrochem. Commun.* **2007**, *9* (9), 2256−2260.
(32) Kumar, A.; Ramani, V. *J. Electrochem. Soc.* **2013**, *160* (11), F1207−F1215.
(33) Li, X.; Guo, Z.; He, T. *Phys. Chem. Chem. Phys.* **2013**, *15* (46), 20037−20045.
(34) Ho, V. T. T.; Pan, C.-J.; Rick, J.; Su, W.-N.; Hwang, B.-J. *J. Am. Chem. Soc.* **2011**, *133* (30), 11716−11724.
(35) (a) Haas, O. E.; Briskeby, S. T.; Kongstein, O. E.; Tsypkin, M.; Tunold, R.; Boerresen, B. T. *J. New Mater. Electrochem. Syst.* **2008**, *11*, 9−14. (b) Thanh Ho, V. T.; Pillai, K. C.; Chou, H.-L.; Pan, C.-J.; Rick, J.; Su, W.-N.; Hwang, B.-J.; Lee, J.-F.; Sheu, H.-S.; Chuang, W.-T. *Energy Environ. Sci.* **2011**, *4* (10), 4194−4200.
(36) Kuvarega, A. T.; Krause, R. W. M.; Mamba, B. B. *J. Nanosci. Nanotechnol.* **2013**, *13* (7), 5017−5027.
(37) Sui, R.; Young, J. L.; Berlinguette, C. P. *J. Mater. Chem.* **2010**, *20* (3), 498−503.
(38) Gasteiger, H. A.; Kocha, S. S.; Sompalli, B.; Wagner, F. T. *Appl. Catal., B* **2005**, *56* (1−2), 9−35.
(39) Sun, S.; Zhang, G.; Sun, X.; Cai, M.; Ruthkosky, M. *J. Nanotechnol.* **2012**, *2012*, 8.
(40) Garsany, Y.; Baturina, O. A.; Swider-Lyons, K. E.; Kocha, S. S. *Anal. Chem.* **2010**, *82* (15), 6321−6328.
(41) Traversa, E.; Di Vona, M. L.; Licoccia, S.; Sacerdoti, M.; Carotta, M. C.; Gallana, M.; Martinelli, G. *J. Sol−Gel Sci. Technol.* **2000**, *19* (1), 193−196.
(42) Feng, X.; Shankar, K.; Paulose, M.; Grimes, C. A. *Angew. Chem., Int. Ed.* **2009**, *48* (43), 8095−8098.
(43) Gaikwad, A. B.; Navale, S. C.; Ravi, V. *Mater. Sci. Eng., B* **2005**, *123* (1), 50−52.
(44) Lewera, A.; Timperman, L.; Roguska, A.; Alonso-Vante, N. *J. Phys. Chem. C* **2011**, *115*, 20153−20159.
(45) (a) Xiong, L.; Manthiram, A. *Electrochim. Acta* **2004**, *49* (24), 4163−4170. (b) Mentus, S. V. *Electrochim. Acta* **2005**, *50* (18), 3609−3615.
(46) Anh Huy, H.; Aradi, B.; Frauenheim, T.; Deák, P. *J. Appl. Phys.* **2012**, *112 (1)* (016103), 016101−016103.
(47) (a) Yang, B.; Lu, Q.; Wang, Y.; Zhuang, L.; Lu, J.; Liu, P.; Wang, J.; Wang, R. *Chem. Mater.* **2003**, *15* (18), 3552−3557. (b) Wang, D.; Zhuang, L.; Lu, J. *J. Phys. Chem. C* **2007**, *111* (44), 16416−16422.
(48) Kropf, A. J.; Katsoudas, J.; Chattopadhyay, S.; Shibata, T.; Lang, E. A.; Zyryanov, V. N.; Ravel, B.; McIvor, K.; Kemner, K. M.; Scheckel, K. G.; Bare, S. R.; Terry, J.; Kelly, S. D.; Bunker, B. A.; Segre, C. U. *AIP Conf. Proc.* **2010**, *1234*, 299−302.
(49) Ravel, B.; Newville, M. *J. Synchrotron Radiat.* **2005**, *12* (4), 537−541.
(50) Wang, C.; Dale, N.; Adjemian, K. *ECS Trans.* **2011**, *41*, 2245−2253.
(51) (a) Tauster, S. J. *Acc. Chem. Res.* **1987**, *20*, 389−394. (b) Lewera, A.; Timperman, L.; Roguska, A.; Alonso-Vante, N. *J. Phys. Chem. C* **2011**, *115* (41), 20153−20159.
(52) (a) Horsley, J. A. *J. Am. Chem. Soc.* **1979**, *101* (11), 2870−2874. (b) Chen, B. H.; White, J. M. *J. Phys. Chem.* **1982**, *86* (18), 3534−3541.
(53) Shim, J.; Lee, C.-R.; Lee, H.-K.; Lee, J.-S.; Cairns, E. J. *J. Power Sources* **2001**, *102* (1−2), 172−177.
(54) (a) Sambandam, S.; Ramani, V. *Phys. Chem. Chem. Phys.* **2010**, *12*, 6140−6149. (b) Williams, M. V.; Kunz, H. R.; Fenton, J. M. *J. Electrochem. Soc.* **2005**, *152*, A635−A644.
(55) Fleischmann, M.; Koryta, J.; Thirsk, H. R. *Trans. Faraday Soc.* **1967**, *63* (0), 1261−1268.
(56) Boudart, M.; Vannice, M. A.; Benson, J. E. *Z. Phys. Chem. (Frankfurt am Main)* **1969**, *64*, 171−177.
(57) Yasuda, K.; Taniguchi, A.; Akita, T.; Ioroi, T.; Siroma, Z. *Phys. Chem. Chem. Phys.* **2006**, *8* (6), 746−752.